Folic acid conjugated polymer as a nano-carrier: dual targeting of tumor cells and tumor microenvironment

by

Pearl Moharil

B.Tech., Vellore Institute of Technology, 2017

Submitted to the Graduate Faculty of

School of Pharmacy in partial fulfillment

of the requirements for the degree of

Master of Science

University of Pittsburgh

2019

UNIVERSITY OF PITTSBURGH

SCHOOL OF PHARMACY

This thesis/dissertation was presented

by

Pearl Moharil

It was defended on

March 29, 2019

and approved by

Dr. Song Li, Professor, Pharmaceutical Science

Dr. Da Yang, Assistant Professor, Pharmaceutical Science

Dr. Vinayak Sant, Assistant Professor, Pharmaceutical Science

Thesis Advisor/Dissertation Director: Dr. Song Li, Professor, Pharmaceutical Science

Folic acid conjugated polymer as a nano-carrier: dual targeting of tumor cells and tumor microenvironment

Pearl Moharil, B.Tech

University of Pittsburgh, 2019

Polymeric micelles have been extensively used in pharmaceutical research for drug delivery. However, most polymeric systems have sizes above 100 nm, which may limit effective extravasation into tumors that are poorly vascularized and have dense stroma. In this project, we synthesized a pVBSS backbone and conjugated it with Gemcitabine (GEM) via a disulfide bond. This system was then used to load Doxorubicin (DOX), for co-delivery of GEM and DOX to tumor cells. We hypothesize that the cellular uptake of pVBSS-GEM can be enhanced by conjugating a targeting ligand, such as folate (FA), to the polymer backbone. This could actively target the FR, which is overexpressed not only on several types of cancer cells but also on the tumor-associated M2 macrophages present in the microenvironment.

FA-pVBSS-GEM/DOX was successfully synthesized and it formed small spherical micelles of 10 nm diameter. The targeting micelle showed a sustained DOX release profile and successfully increased DOX uptake in 4T1.2 and KB cells in vitro. In vivo, systemic delivery of FA-pVBSS-GEM/DOX led to higher micellar accumulation in the tumor environment and remarkably reduced the tumor growth in a murine 4T1.2 breast cancer model.

Table of Contents

List of Tables

List of Figures

List of Schemes

1.0 INTRODUCTION

1.1 **Cancer Therapeutics**

Breast cancer is one of the most common cancer malignancies affecting women worldwide with 255,180 new cases reported in 2017 in the US alone (1). With the number rising each year, the standard treatments used for these patients is mostly restricted to chemotherapy, radiation, or surgical removal of the gland, also known as mammoplasty. Even though hormone and Her-2 based antibodies are available for a certain population of breast cancer patients, no viable treatments are available for triple negative breast cancer. Currently, there are more than 70 antineoplastic drugs developed and used in clinical settings. However, they are usually associated with high toxicity, poor solubility, and high clearance (2).

Doxorubicin (DOX), a hydrophobic compound, is one of the most common anticancer drugs used to treat several cancer types. It is believed that DOX exhibits its activity through cellular DNA damage by inhibiting topoisomerase II and generating free radicals via redox reactions (3, 4). Often used in combination therapy, this drug is on the World Health Organization's essential medicines list. Despite its well-established activity, cardiomyopathy remains the most common and most dangerous side effect of DOX. To counter these effects, PEGylated and liposomal formulations of DOX, such as Doxil are now commercially available (5). Another anticancer drug, Gemcitabine (GEM) is a hydrophilic molecule that can also induce DNA damage to rapidly dividing cells. It is widely used clinically against a variety of solid tumors (6). However, adverse

effects such as bone marrow suppression and contraindications, are commonly associated with the administration of this drug.

1.2 **Polymeric micelles as drug delivery systems**

Although these small molecular drugs are highly associated with the antitumor activity, they tend to damage both cancerous and normal cells alike due to their unbiased distribution post administration, inducing toxicity in patients. Many chemotherapeutic molecules are also poorly water-soluble, with a limited number of formulations approaches available. For such drugs, encapsulation in surfactants such as CrEL have been designed, but are associated with a variety of side-effects (flushing, anaphylaxis) in patients. In recent years, many nanocarriers such as polymers, liposomes, and dendrimers have also been established for drug delivery as well as non-invasive imaging (7-9). Polymers, when designed and synthesized to be amphipathic, can readily self-assemble to form spherical micelles in the presence of an aqueous phase. Polyethylene glycol (PEG), poly(D,L-lactic-co-glycolic acid) PLGA, PEG-PLA-, and PEG-PCL-based micelle systems have previously demonstrated high efficiency in delivering hydrophobic as well as hydrophilic drugs (10, 11). These polymers can be tailored easily to obtain good compatibility with drugs. Then the drugs can be either chemically conjugated to these polymer backbones or loaded within the micelles, or both.

Delivering drugs through such micelles can pose several advantages. The relatively nonpolar and hydrophobic core is suitable for loading poorly soluble hydrophobic drugs, which are difficult to formulate. (10, 12). In vitro and in vivo, such micelles systems have demonstrated a sustained drug release profile, increasing the therapeutic effect of the drug. The process of

opsonization has been described as one of the most important biological barriers to drug delivery. PEG is known to block protein and cell surface interactions, which greatly decreases nanoparticle uptake by the reticuloendothelial system (RES) and consequently avoid fast clearance of these micelles (13, 14). However, the size of most micelles currently in research is around 100 nm in diameter. Such systems can achieve high drug loading capacity but cannot effectively enter or infiltrate the tumor microenvironment. Due to these concerns, we aim to synthesize nanoparticles of a size of 10 to 20 nm diameter as it is large enough to avoid biological clearance and small enough to penetrate tumor vasculature (15). Moreover, the tumor environment lacks lymphatic vessels, which can cause an accumulation of micelles at the tumor site (16). This passive targeting of tumors, known as the enhanced permeability and retention (EPR) effect, can help reduce systemic toxicities of chemotherapeutic drugs.

1.3 **Active Targeting**

To achieve greater specificity towards cancer cells, distinct cellular physiologies of cancerous cells, such as vasculature and hypoxia, have been studied extensively (12). In order to increase therapeutic efficiency, nanoparticles have been conjugated with numerous targeting ligands to specifically target tumor cells and enter via receptor-mediated endocytosis. Among these, folic acid has been well studied and poses advantages such as non-immunogenicity and small size (17-19). Folic acid (FA) is a form of vitamin B, required by cells for their survival and proliferation. It is involved in the carbon methyl transfer reaction of de novo purine synthesis and is an essential part of the nucleic acid synthesis (20). It is safe to say that cells cannot divide efficiently without FA as the synthesis of new DNA/RNA strands is impaired (21). FA and FA-

conjugates bind and be endocytosed into the cells via folate receptors (FR), a type of G protein-coupled receptors (GPCR) (22-24). Notably, FA can retain a high affinity for the receptor post derivation via its γ-carboxylic acid group. There are four different isoforms of FR currently known: FRα, FRβ, FRγ, and FRδ. Out of these, the most prevalent and common isoforms relative to therapeutic potential are FRα and FRβ (25). FRα, the dominant isoform, is present on the apical surface of epithelial cells of mammary ducts, lungs, and kidney.

1.3.1 **Targeting FRα**

Altogether, studies strongly indicate that FRα overexpression is observed in about 40% human cancer types, with 90 to 95% ovarian cancer cases overexpressing the receptor (26-28). As a result, site-specific targeting of FR is not unfamiliar and has been extensively studied for its therapeutic potential (29-33). In vitro, FA conjugation to liposomes and micelles for active targeting, successfully improved uptake and cytotoxic effect of drugs in cells overexpressing FR (34-36). These FA-conjugated micelles have been extensively used for delivery of DOX, PTX, Curcumin, and other drugs, resulting in significantly reduced tumor growth and metastasis in murine cancer models, (when compared to non-targeting micelles) (13, 37-42). Vintafolide, folate conjugated therapeutic, and Farletuzumab, a monoclonal antibody are currently in phase I clinical trials targeting FR of solid tumors. More recently, vintafolide entered phase II trial as a combination therapy with pegylated liposomal doxorubicin in patients diagnosed with platinum-resistant ovarian cancer. Additionally, FR targeting nanoparticles have been used to image patients for identification of FRα positive tumors (43).

1.3.2 **Targeting FRβ**

FRβ, on the other hand, has recently come into light due to its expression on myeloid cells. The receptor has been associated with macrophages, specifically the tumor associated macrophages (TAMs), suggesting its involvement in cell growth and metastasis (44, 45). The M2 phenotype is well associated with angiogenesis, high arginase, and mannose receptor expression, and other tumor progressing events (46, 47). Several groups report that FRβ is expressed exclusively on (alternatively activated) M2 macrophages as compared to (classically activated) M1 type (48, 49), and targeting them via FRβ specific antibodies have shown benefit in tumor regression studies (50). This is particularly interesting as these macrophages could be possible targets of folate-drug conjugates.

1.4 **Aims and Hypotheses**

Keeping in view the current drawbacks and limitations of anticancer drugs and polymeric micelles, our lab functionalized a polymer backbone conjugated with GEM to form highly stable micelles of small size. GEM could be conjugated via reduction sensitive disulphide bond, that can maintain the stability of formulation and be cleaved at the tumor site to release the drug. These micelles can successfully load several anticancer drugs and show good stability at pH 7. The aim of this research is to further enhance the cellular uptake of such drug-loaded micelles by conjugating ligands, such as folate, to target the tumor cells. Thus, the passive EPR effect and active FR targeting could synergistically improve the therapeutic activity of our micelle system.

We hypothesize that the delivery of DOX via FA-conjugated micelles targeting FR could enhance the antitumor effect of DOX, increase specificity and limit the off-target adverse side effects.

2.0 MATERIALS AND METHODS

2.1 **Materials**

2.1.1 **Reagents**

Doxorubicin hydrochloride (DOX·HCl) was obtained from LC Laboratories (MA, USA). Vinylbenzyl chloride, potassium carbonate (K_2CO_3), azobisisobutyronitrile (AIBN), petroleum ether (PE), sodium hydroxide (NaOH), 2-hydroxyethyl methacrylate, di-tert-butyl dicarbonate, 1,4-Dioxane, dimethylformamide (DMF), tetrahydrofuran (THF), dimethyl sulfoxide (DMSO), triethylamine (TEA), 4-cyano-4-[(dodecylsulfanylthiocarbonyl) sulfanyl] pentanoic acid, poly(ethylene glycol) (PEG2K), and poly(ethylene glycol) methyl ether methacrylate (OEGMA) were purchased from Fisher Scientific.

2.1.2 **Cell lines**

KB cells were obtained from Dr. Larry Matherly at Ann Karmanos, Michigan. 4T1.2 and RAW 264.7 cells were obtained from ATCC (Manassas, VA). All the cell lines were routinely cultured in Roswell Park Memorial Institute (RPMI) 1640 Medium supplemented with 10% fetal bovine serum (FBS) and 1% penicillin-streptomycin at 37℃ in a humidified environment with 5% CO_2.

2.1.3 **Animals**

The female BALB/c mice (5-6 weeks) of 18-20 g weight were purchased from Charles River (Davis, CA, USA). The animal protocols were approved by the Animal Use and Care Administrative Advisory Committee at the University of Pittsburgh. The mice were housed under pathogen-free conditions and all experimental studies were completed according to the guidelines approved by the Ethics Committee of the University of Pittsburgh.

2.2 **Synthetic Schemes**

2.2.1 **Synthesis of pVBSS**

To obtain a batch of VBSS monomer, 2.3 g dithiodibutyric acid was stirred with 0.3 mL Vinyl benzyl chloride and 1 g K_2CO_3 overnight at 50°C. The monomer was dissolved in dichloromethane and extracted from the solution by centrifugation. The supernatant was collected and extracted from the solution twice with water followed by extraction with saline. Next, it was dried over anhydrous sodium sulfate for 20 min and purified by flash column chromatography (ethyl acetate and petroleum ether used in 1:3 ratio). The separation was monitored by thin layer chromatography and the final product was confirmed via NMR.

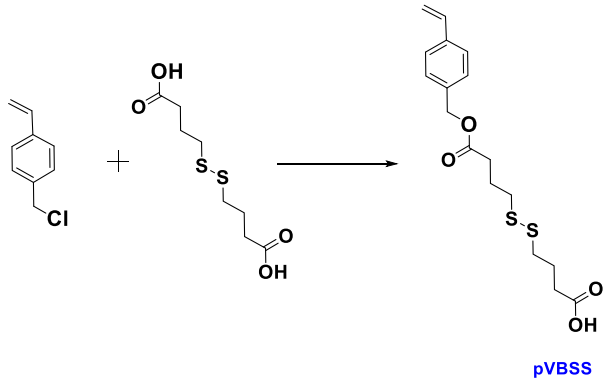

Scheme 1:Synthesis of pVBSS

After obtaining pure monomer, it was mixed with PEG_{950} and AIBN in the presence of RAFT reagent and 1 mL THF. The mixture was then added to a Schlenk tube and purged with nitrogen in order to remove the oxygen dissolved in the reaction solvent by using a freeze-pump-thawing method. Briefly, the solution was frozen in liquid nitrogen under a vacuum environment for 10 min and then exposed to room temperature nitrogen air flow for 10 min. The cycle was repeated thrice after which, the tube was immersed in an oil bath at 85℃ overnight under nitrogen protection. The pVBSS polymer was then purified by precipitation using cold diether thrice. The final polymer solution was dried in a vacuum pump and the structure was confirmed by proton NMR.

2.2.2 **Synthesis of pVBSS-GEM**

The polymer pVBSS was reacted with EDC.HCL, HOBT, DIPEA, and Gemcitabine (GEM) in 5 mL DMSO. The reaction was maintained at 37 °C for 72 hours, following which the solution was dialyzed against ultrapure water for two days at room temperature. The obtained

solution was filtered through a syringe filter (pore size = 0.45µm), frozen at -80 °C and then freeze-dried in a lyophilizer overnight. The polymer was dissolved in dichloromethane at 35 mg/mL.

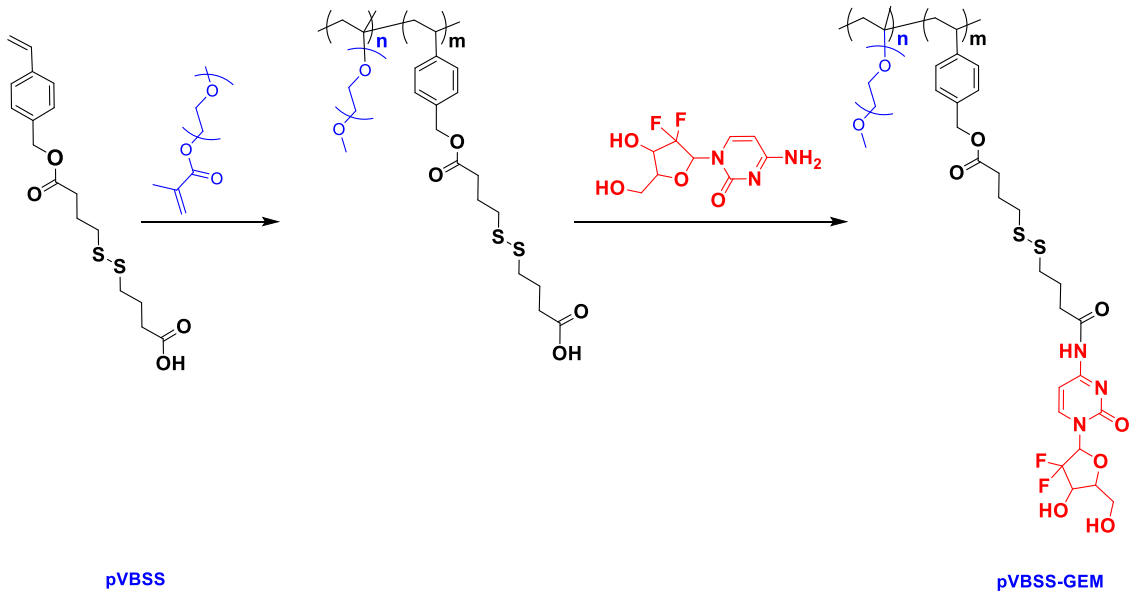

Scheme 2: Synthesis of pVBSS-GEM

2.2.3 **Synthesis of FA-pVBSS-GEM**

To obtain a folate-conjugated polymer, a slight modification was employed. Instead of $PEG_{950,}$ NH_2-PEG_{5K}-NH_2 was initially conjugated with folic acid. The longer PEG spacer is used to ensure that the folic acid is accessible as a targeting ligand to folate receptor overexpressing cells. This moiety was then linked to the pVBSS polymer in the presence of EDC.HCL, HOBT, DIPEA, and Gemcitabine. After stirring the reaction in 5 ml DMSO at 37 °C for 72 hours, it was dialyzed against water for two days. The solution obtained was filtered, frozen at -80 °C and then

freeze-dried overnight in a lyophilizer. The final solution was soluble at a concentration of 26 mg/mL in dichloromethane.

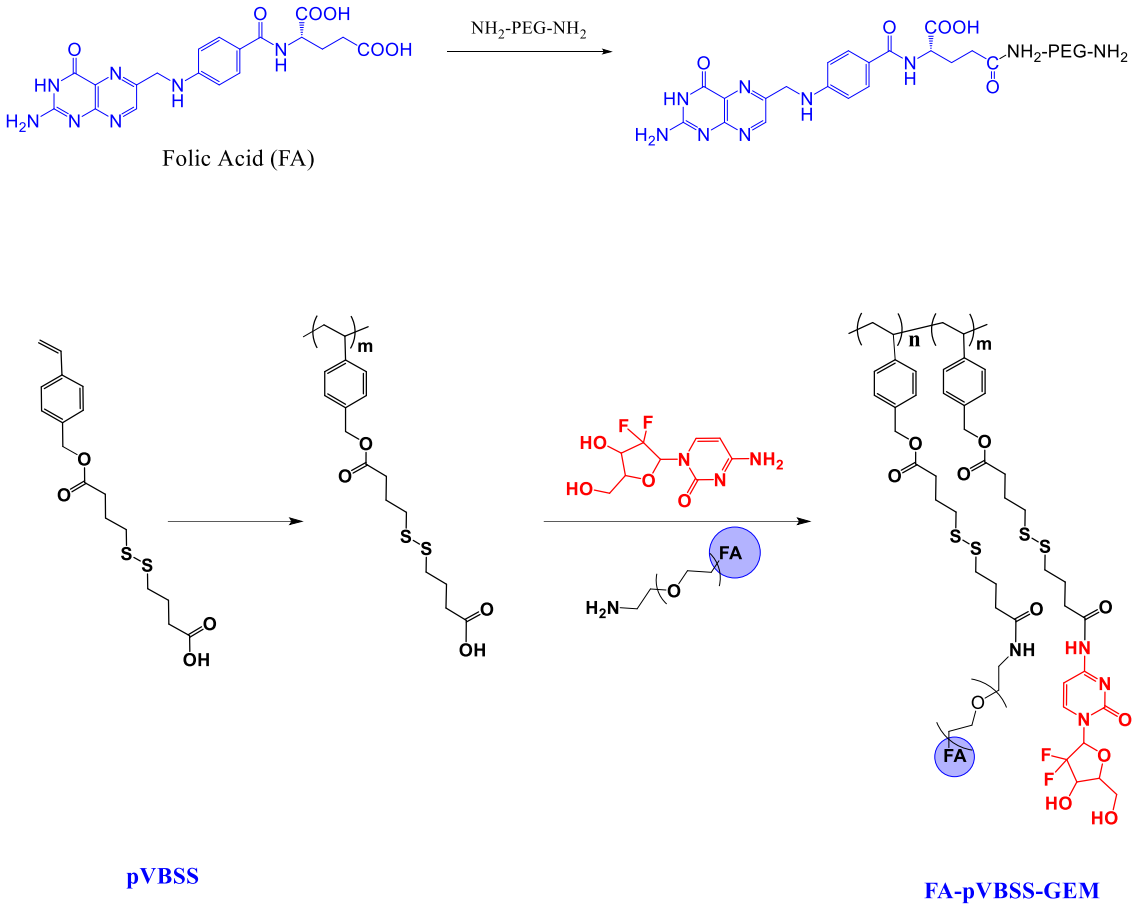

Scheme 3: Synthesis of FA-pVBSS-GEM

2.3 Preparation of DOX-free and DOX-loaded micelles

DOX·HCl was first neutralized by 3 mol equivalent of triethylamine in $CHCl_3$/MeOH (1:1. v:v) to remove HCl. The pVBSS-PEG_{950}-GEM and FA-pVBSS-PEG_{5K}-GEM polymers were mixed in different ratios to obtain 1 mg of the mixed polymer solution. To this, 20 µL of 5 mg/ml DOX was added and the final solution was air-dried to obtain a film (DOX/polymer:1/10, w/w).

After removing all solvent in a vacuum pump, fresh PBS was added to hydrate the film, forming DOX-loaded mixed micelles. Solutions were filtered through a syringe filter (pore size = 0.45 μm) to remove unloaded DOX. Blank micelles were prepared similarly without adding DOX.

2.4 **Characterization of micelles**

The mean hydrodynamic diameter, size distribution, and zeta potential of various formulations of micelles were evaluated by dynamic light scattering (DLS) after a 0.45μm filtration. For the morphological analysis of blank and DOX-loaded micelles, low concertation solutions were observed under transmission electron microscopy (TEM). To evaluate the drug loading efficiency and capacity, micelles were dissolved in DMSO to break the micelle structure and release DOX. The concentration of DOX-loaded in the micelles was determined by UV Spectrometer (excitation 490 nm/emission 600 nm) using a calibration curve. The drug loading efficiency (DLE) was calculated with respect to the following formula:

DLE (%) = (Weight of Loaded Drug / Weight of Input Drug) x 100

The critical micellar concentration (CMC) of FA-pVBSS-PEG_{5K}-GEM was determined using Nile red as a fluorescent probe. 20 μL of 1.5 mg of Nile red in dichloromethane was added to twenty tubes and incubated in a dark room overnight at room temperature to remove the solvent. Next, 2 mL of FA-pVBSS-PEG_{5K}-GEM micellar solution was added at logarithmic dilutions to each tube. Post 6 h, the emission spectra of the solutions were measured (excitation wavelength of 550 nm and emission of 650 nm) and recorded. The absorbance values were plotted, and the CMC concentration was calculated at the intersection point of two slopes.

2.5 **DOX release kinetics**

The pVBSS-GEM/DOX and FA-pVBSS-GEM/DOX micelle systems were tested for their in vitro release kinetics of DOX. For this experiment, 50 mL PBS (pH = 7.4) was used as the release medium and free DOX was employed as a control. In short, 250 µL of DOX-loaded micelles (5 mg DOX/mL) was sealed in dialysis bags (MWCO = 3.5 kDa). The dialysis bags were immersed in 50 mL PBS release medium in a beaker covered with Parafilm. The beakers were kept in an incubator shaker at 100 rpm and 37 °C. At pre-determined time points, 1 mL of external buffer was collected and replaced with 1 mL fresh PBS. The concentration of DOX in collected tubes, was measured by UV Spectrophotometer with the fluorescence detected at 580 nm. Error bars were obtained from triplicate samples.

2.6 **FR expression in cell lines**

To evaluate the FRα and FRβ expression in 4T1.2 and KB cell lines, the cell were plated at high confluency in RPMI-1640 medium and cultured overnight. Their RNA was isolated, retrotranscribed and amplified using standard procedures. Oligonucleotide sequences for murine FOLR1: (PF) 5’ GTGTCACAGGATTCAGGCCA 3’; (PR) 5’ TCGGGCTTCTTTGTCTCCAC3’, FOLR2: (PF) GTCACTTCATCCAAGACTCCTGC; (PR) CACTGGTGACAGTCCTCTTTGC and GAPDH: (PF) 5’ AGG TTG TCT CCT GCG ACT TCA 3’; (PR) 5’ TGG TCC AGG GTT TCT TAC TCC 3’. Primers specific for KB FOLR1, FOLR2: (PF) 5’ CATGTGCAGTGCCCAGGA 3’; (PR) 5’ CCAGGGACTGCATTGGTCAT 3’ and

GAPDH (PF) 5’ GCACCGTCAAGGCTGAGAAC 3’; (PR) 5’ TGGTGAAGACGCCAGTGGA 3’.

2.7 **In vitro cytotoxicity assay**

4T1.2 and KB cells were plated in a 96-well plate and cultured overnight at 37 °C with 5% CO_2. Next, the cells were treated with DOX, pVBSS-GEM, pVBSS-GEM/DOX, FA-pVBSS-GEM, FA-pVBSS-GEM/DOX and FA-pVBSS-GEM/DOX in the presence of free folate (1mM) (1:100 v/v) in the media at various dilutions for 30 min. Following a 24 hours incubation, the media from each well was replaced with 100µL MTT reagent (10 %) and incubated for an additional 4 hours. Finally, the MTT reagent was replaced by 100µL of filtered DMSO to dissolve the formalin crystals, giving rise to a purple colored solution. The absorbance for the plate was recorded using a UV Spectrophotometer and % cellular viability was calculated as (($OD_{treated} - OD_{blank}$) x 100%).

2.8 **Cellular uptake study**

A total of 3×10^5 KB and 4T1.2 cells were seeded into each well of 6-well plates and grown overnight at 37 °C and 5% CO_2 conditions. The medium was replaced by fresh Folate-free RPMI 1640 medium containing free DOX, pVBSS-GEM/DOX, FA-pVBSS-GEM/DOX, and FA-pVBSS-GEM/DOX in the presence of 1mM free folic acid for 30 min. Each formulation was prepared fresh at an equivalent DOX concentration of 6 µg/mL. The cells were incubated for 30

min at 37 °C, and then washed three times with cold PBS and fixed with 10% paraformaldehyde solution for 10 min on ice. Following fixation, the wells were washed with cold PBS thrice. Next, the nuclei were stained with DAPI for 5 min and wells were again washed three times with cold PBS. Finally, the intracellular uptake of DOX in various formulations was observed under fluorescence microscopy.

For further quantification of the DOX uptake, KB and 4T1.2 cells were seeded in a 6-well plate at a high density ($1x10^6$ cells/well) and incubated overnight at 37 °C and 5% CO_2. The medium by replaced by a 2 ml solution of fresh Folate-free RPMI 1640 medium containing Free DOX, pVBSS-GEM/DOX, FA-pVBSS-GEM/DOX, and FA-pVBSS-GEM/DOX in the presence of 1mM free folic acid for 30 min. The formulations were prepared to keep an equivalent DOX concentration of 6 μg/mL. Next, the medium was removed, and cells were washed three times with 1mL cold PBS. The cells were harvested with 0.5 mL trypsin treatment and centrifuged at high speed. The cell pellet obtained was washed with 1 mL of PBS three times to remove traces of cell culture media. Next, the cells were fixed in solution using 10% paraformaldehyde solution for 10 min. Following a brief spin down, the cells were washed with 1 mL PBS twice. Finally, the cell pellet was suspended in 200 μL PBS and transferred to the flow cytometry tubes for the flow cytometry analysis with MACS Quant Analyzer. A total of 20000 events were collected for each sample. The DOX uptake in cells was excited with an argon laser (480 nm), and fluorescence was detected at 570 nm.

2.9 **Biodistribution of dox in vivo**

Four female BALB/c mice were inoculated with $2x10^5$ 4T1.2 cells/ mice and the tumor size was observed daily. After a large tumor volume was achieved, the mice were randomly assigned to two different treatment groups (n=2). The groups received single i.v. dose of free DOX, pVBSS-GEM/DOX, and FA-pVBSS-GEM/DOX with the DOX concentration maintained at 10 mg/kg. 24 hours post administration, the mice were sacrificed, and their tumor and other major organs were harvested.

To observe DOX uptake in tumors, frozen sections of 10 µm thickness were collected using CryoStar NX50. The slides were fixed with 10% formalin for 10 min, following a wash with cold PBS three times. Finally, a mounting solution with DAPI was added and the slides were covered with coverslips. The frozen sections were observed for their DOX uptake signal under a fluorescence microscope.

2.10 **In vivo near-infrared fluorescence (NIRF) optical imaging**

$2x10^5$ 4T1.2 cells/ mice were inoculated subcutaneously at the left flank of six female BALB/c mice and the tumor size was monitored daily. Once the tumor volume reached 50−100 mm^3, mice were randomly assigned to three different groups (n=2). The three groups received an i.v. injection of DIR, pVBSS-GEM/DIR, and FA-pVBSS-GEM/DIR respectively. The polymer to DIR ratio was maintained at 20:1 for all formulations. Post 24 hours, the mice were euthanized, and their tumors and major organs were excised and scanned for ex-vivo imaging using an IVIS Imaging system with excitation at 750 nm and emission at 780 nm (exposure time of 60 sec was

used). By measuring the signal intensities, the distribution of DIR through these micelles in different tissues was quantified.

2.11 **In vivo antitumor efficacy study**

$2x10^5$ 4T1.2 cells were inoculated in 30 female BALB/c mice and the tumor size was observed daily. Once the tumor reached a volume of 50-100 mm^3, the mice were randomly divided into seven groups and numbered. Next, the groups received three i.v. tail injection doses of Saline, DOX, pVBSS-GEM, FA-pVBSS-GEM, and FA-pVBSS-GEM/DOX on days 1, 4, and 7. The DOX concentration was maintained at 5 mg/kg body weight. The tumor volume, measured with a digital caliper, was recorded on days 1, 4, 7, 10, 13, and 16 using the formula (L ×W2)/2, where L and W are length and width of each tumor respectively. To compare the various groups, relative tumor volume (RTV) was calculated, where RTV = (tumor volume at a given time point/initial tumor volume). Additionally, the body weight of all mice was recorded to monitor toxicity. The tumor growth inhibition rate (IR) was also assessed by calculating IR % = (1 - RTV in the treated group/RTV in the saline group) × 100%.

2.11.1 **Safety evaluations**

Once the tumor volume reached 2000 mm^3, the mice were sacrificed, and their tumor and other major organs were excised, including fresh blood samples. The blood serum was used to analyze and measure aspartate aminotransferase (AST) and alanine aminotransferase (ALT) enzyme activity as biomarkers for liver toxicity. The organs were fixed with 4% (v/v)

paraformaldehyde in PBS (PH 7.4), embedded in paraffin, and sectioned into 4 µm slices. Each section was processed for H&E, and TUNEL staining and observed under a microscope. Immunohistochemical analysis (IHC) of Ki67 protein, an important biomarker of cell proliferation and breast cancer repression, was carried out using the labeled streptavidin-biotin method. Ki67 expression was quantified by calculating the number of Ki-67 positive cells/total number of cells in five randomly selected areas using ImmuneRatio software.

2.12 **FRβ targeting in M2 macrophages**

To test the effect of folate targeting on FRβ cells, we evaluated its expression on M1 and M2 macrophages. For this, PBMCs were isolated from the spleen of healthy mice (5 to 6 weeks old) and cells were incubated at 37°C and 5% CO_2 for six hours in full RPMI medium. Post incubation, the macrophages could be easily separated (due to their property of adherence) from other mononuclear cells and lymphocytes which are suspended in cell culture medium. To induce an M2 polarization, the macrophages were treated with IL-4 (250 ng/mL) and IL-13 (250 ng/mL) for 18 hours (51). To confirm the results, classic markers for each phenotype were tested. Expression of iNOS (M1 marker) and Arginase (M2 marker) was assessed by real-time quantitative polymerase chain reaction (RT-qPCR). Oligonucleotides used for expression of iNOS: (PF) 5'CGAAACGCTTCACTTCCAA 3'; (PR) 5' TGAGCCTATATTGCTGTGGCT 3'and Arginase 1: (PF) 5' AACACGGCAGTGGCTTTAACC 3'; (PR) 5' GGTTTTCATGTGGCGCATTC3'.

To check the FRβ expression on M2 cells, FRβ mouse primer sequences were used: (PF) 5' GTCACTTCATCCAAGACTCCTGC 3'; (PR) 5' CACTGGTGACAGTCCTCTTTGC 3'.

Cellular uptake of Free DOX, pVBSS-GEM/DOX and FA-pVBSS-GEM/DOX was determined using the protocol described previously in section 2.8.

2.13 **Statistical analysis**

Data was processed by GraphPad Prism 7. All values are reported as mean $\pm$ SEM. In all statistical analyses, the significance level was set at a probability of $p < 0.05$. All results were analyzed by student's *t-test* for two groups, and one-way ANOVA for multiple groups.

3.0 RESULTS

3.1 **Micelle characterization**

As a first step to optimizing the ligand density on the micellar carrier, the two polymers FA-pVBSS-GEM and pVBSS-GEM were mixed in various ratios to obtain different percentages of folic acid conjugated pVBSS-GEM micelles. All the micelle systems readily formed small sized particles with the average hydrodynamical diameter of 12 nm (as measured by volume peak by DLS) and a poly-dispersity index of 0.5-0.9 (Table 1). The zeta potential for all the formulations was negative, suggesting that in a neutral pH buffer, individual micelle units would be repelled from each other and not form aggregates. Loading DOX into these micelles did not have any impact on the size or zeta potential. Micelles were stable in PBS for up to two weeks, following which small aggregates could be observed in the solution.

Table 1: Characterization of micelles

FA%	Micelles	Size (d) (nm)	PDI	Zeta potential (mV)	DLE (%)
0%	pVBSS	11.24 $\pm$ 0.24	0.88	-0.32	86.31
	pVBSS/DOX	8.8 $\pm$ 0.96	0.78	-1.14	
5%	FA-pVBSS	11.08 $\pm$ 0.13	0.9	-3.96	82.43
	FA-pVBSS/DOX	9.17 $\pm$ 1.04	0.5	-2.29	

To further confirm these results, the size and morphology of blank and DOX-loaded pVBSS-GEM/DOX and FA- pVBSS-GEM were visualized by TEM. Homogenously distributed micelles of spherical and uniform size were observed under TEM (Figure 1) with the observed size

consistent with that determined by DLS. For this study, we continued with 5 % ligand density FA-pVBSS-GEM mixed micelle as the targeted drug delivery system. If we further increase the FA % density on the carrier, the ligand might not be sterically available to the receptor.

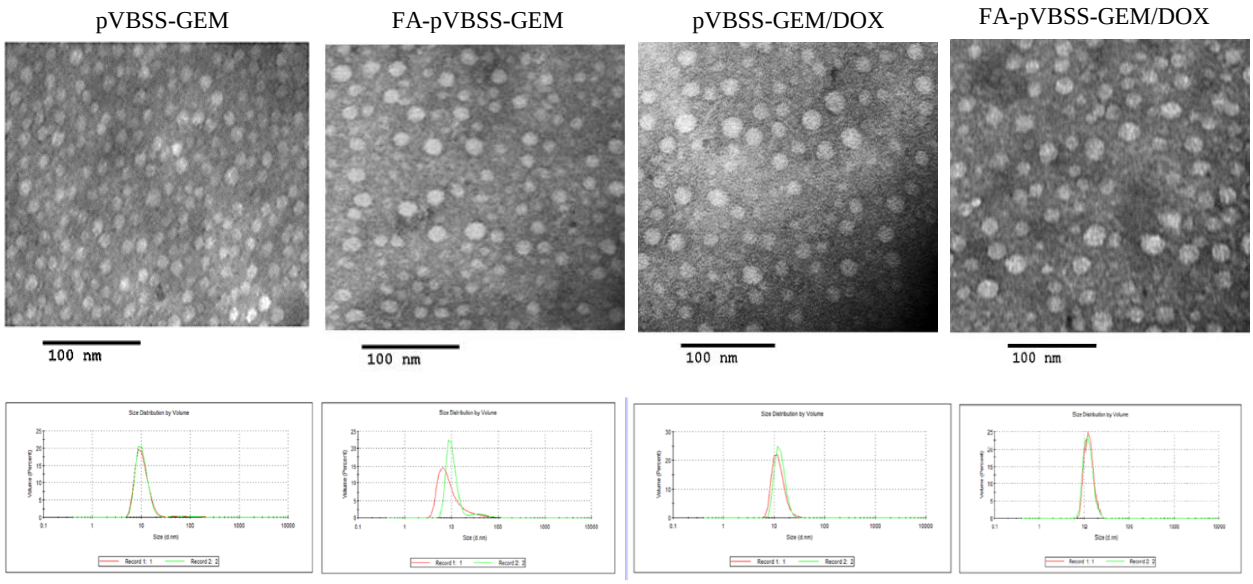

Figure 1: Micelle size and morphology analyzed by TEM (above), and DLS (below)

For in vivo treatment, the formulation will undergo high dilution, once it enters the blood circulation. To check the stability upon dilution, CMC was calculated. CMC of FA-pVBSS-GEM/DOX was established using Nile red as a fluorescence probe and was calculated to be 0.037 mg/mL (Figure 2). The low value indicates that it could provide good stability upon dilution in bloodstream post tail injection.

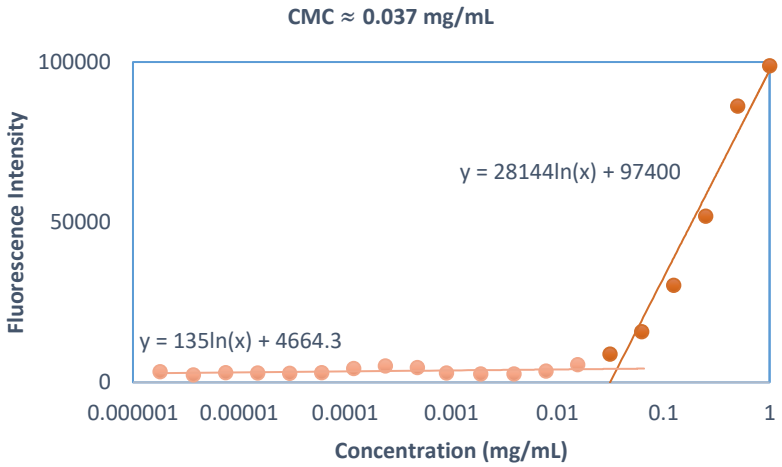

Figure 2: CMC measurement of FA-pVBSS-GEM

3.2 **DOX release kinetics from Micelles**

The release profiles of free DOX and DOX-loaded micelles were tested in PBS (pH 7.4). As expected, free DOX easily diffuses through the dialysis bags and within 12 hours, 80% DOX was found in the release medium. For our micelles, less than 43% DOX was released from micellar cores within 24 hours (Figure 3). This slower and controlled release from the DOX-loaded formulations can be attributed to the strong π–π stacking and hydrophobic interactions between the pVBSS-GEM carrier and DOX.

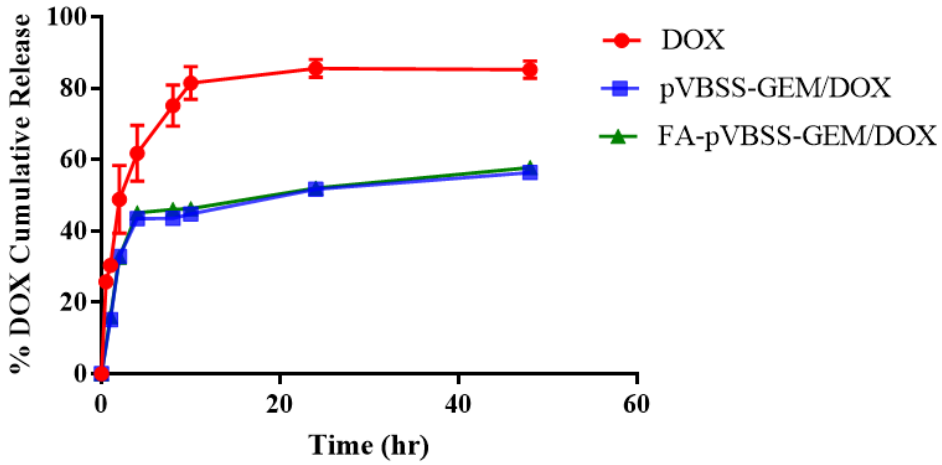

Figure 3: DOX release profiles

3.3 **FR expression in vitro**

The FRα and FRβ expression were evaluated in the 4T1.2 and KB cell lines using the appropriate primer sequences. For both the receptor isoforms, the KB cell line showed a significantly higher expression, concurring with results from other research groups (Figure 4).

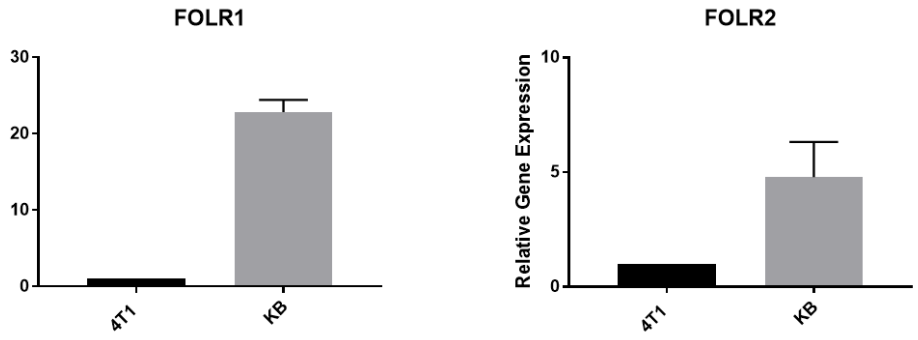

Figure 4: FR isoforms expression levels in 4T1.2 and KB cell lines

3.4 **In vitro cytotoxicity assay**

The cytotoxicity of free DOX, DOX free and loaded pVBSS-GEM and FA-pVBSS-GEM micelles was determined by MTT assay (Figure 5 A, B). While free DOX, pVBSS-GEM, and pVBSS-GEM/DOX micelles inhibited the tumor cell proliferation in a concentration-dependent manner, the benefit of targeting was observed in the FA-conjugated micelles groups. This trend was more significant in KB cells, as compared to 4T1.2 cells. Furthermore, the cytotoxicity of FA-conjugated formulation was essentially blocked by the addition of an excess amount of free FA. The experiment was carried out in triplicates and final % cell viability at 20µg/mL for each formulation is plotted.

A

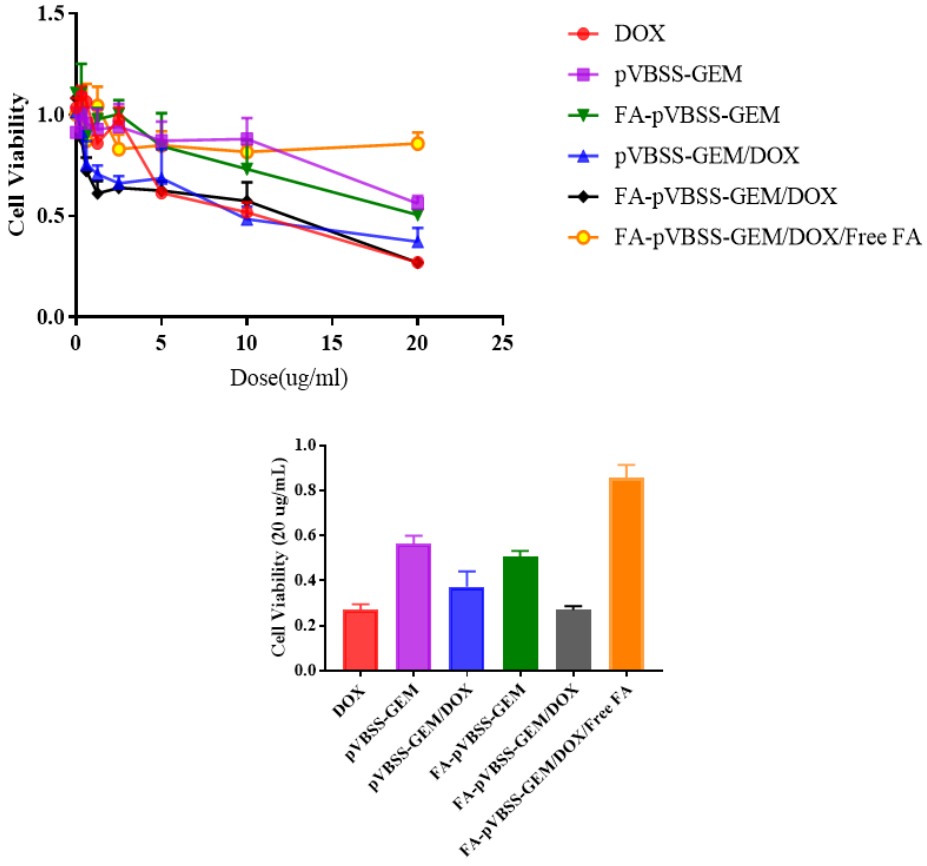

B

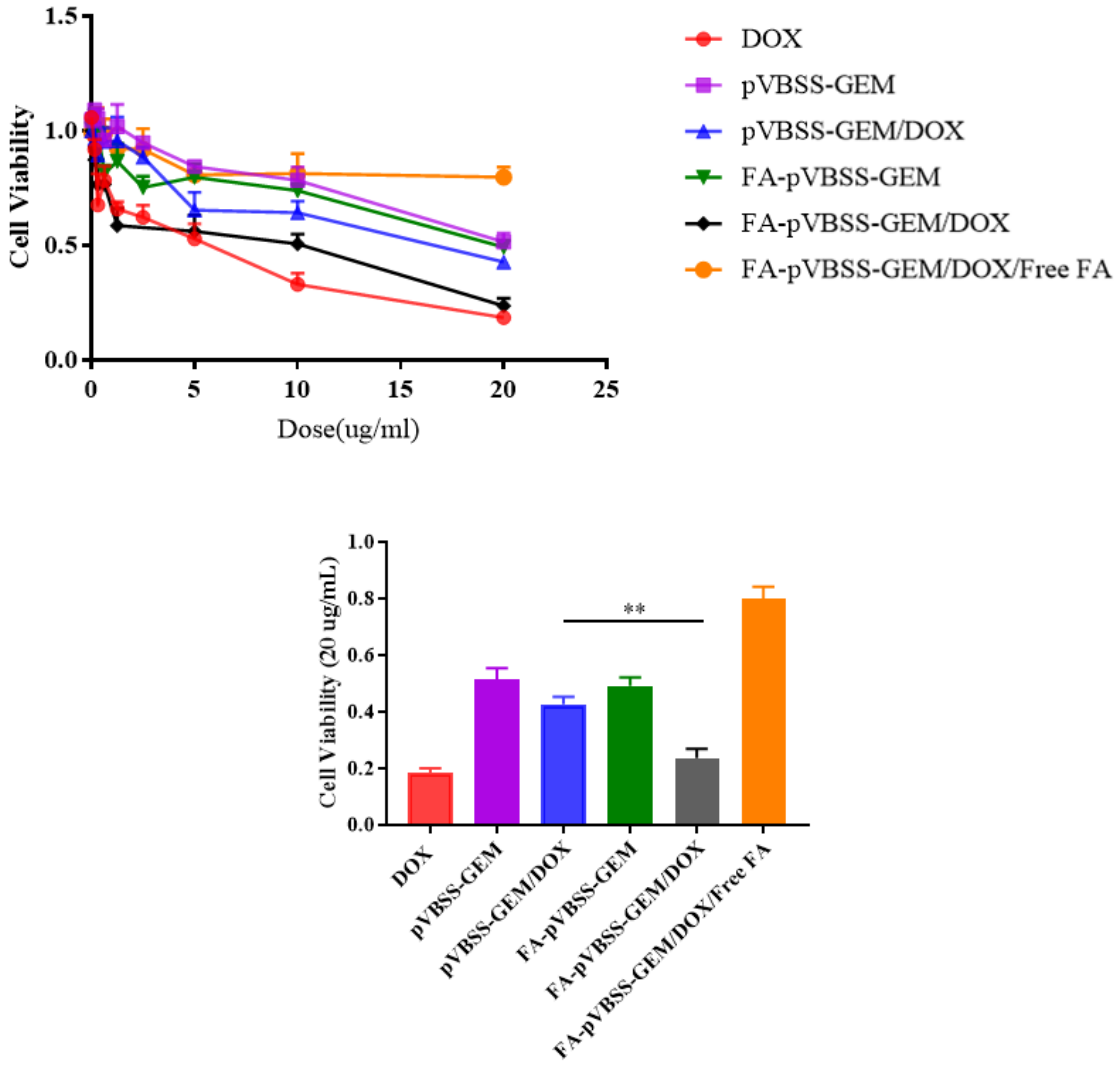

Figure 5: In vitro cytotoxicity assay for (A) 4T1.2 and (B) KB cell lines

3.5 **Cellular uptake study**

To study the uptake of DOX into KB and 4T1.2 cells in vitro, the cell lines were treated with different micelle formulations and assessed for their DOX uptake using a fluorescence

microscope. While the nuclei stained with DAPI appear blue, DOX inherently emits a red fluorescence and this signal can be readily visualized by the microscope. Figure 6 shows the merged images of KB and 4T1.2 cells 30 min post-treatment.

Free DOX could be easily and rapidly taken up by the cells due to its small size and molecular weight and as a result, a high uptake is observed within 30 min of treatment. Importantly, the FA-pVBSS-GEM/DOX showed a greater intensity of red fluorescence as compared to the control pVBSS-GEM/DOX group and free DOX, indicating larger DOX uptake in both cell lines. On adding free folic acid in the media at a concentration of 1 mM, a loss of red fluorescence intensity was observed indicating an inhibition in the uptake of DOX. This competition between folic acid and the FA-conjugated micelles supports the fact that the uptake occurs via folate receptors that are expressed on the surface of these cancer cell lines.

Next, the uptake of DOX into the cells was quantified using flow cytometry as shown in Figure 6. The mean fluorescence intensity (MFI) was measured at 570 nm for KB and 4T1.2 cells, 30 min post-treatment. Free DOX showed an increase in fluorescence intensity. Delivering the drug through a non-targeting polymer reduced the uptake, but after conjugating FA, we see an increase in MFI, which is comparable to free DOX in KB cells. More importantly, the increase of MFI in FA-conjugated treated group was not significant in 4T1.2 cells (which can be attributed to the fact that these cells express a lower expression of FRα as confirmed to KB cells). The MFI was significantly reduced in the presence of excess free FA, confirming the role of folate receptors in targeted DOX uptake.

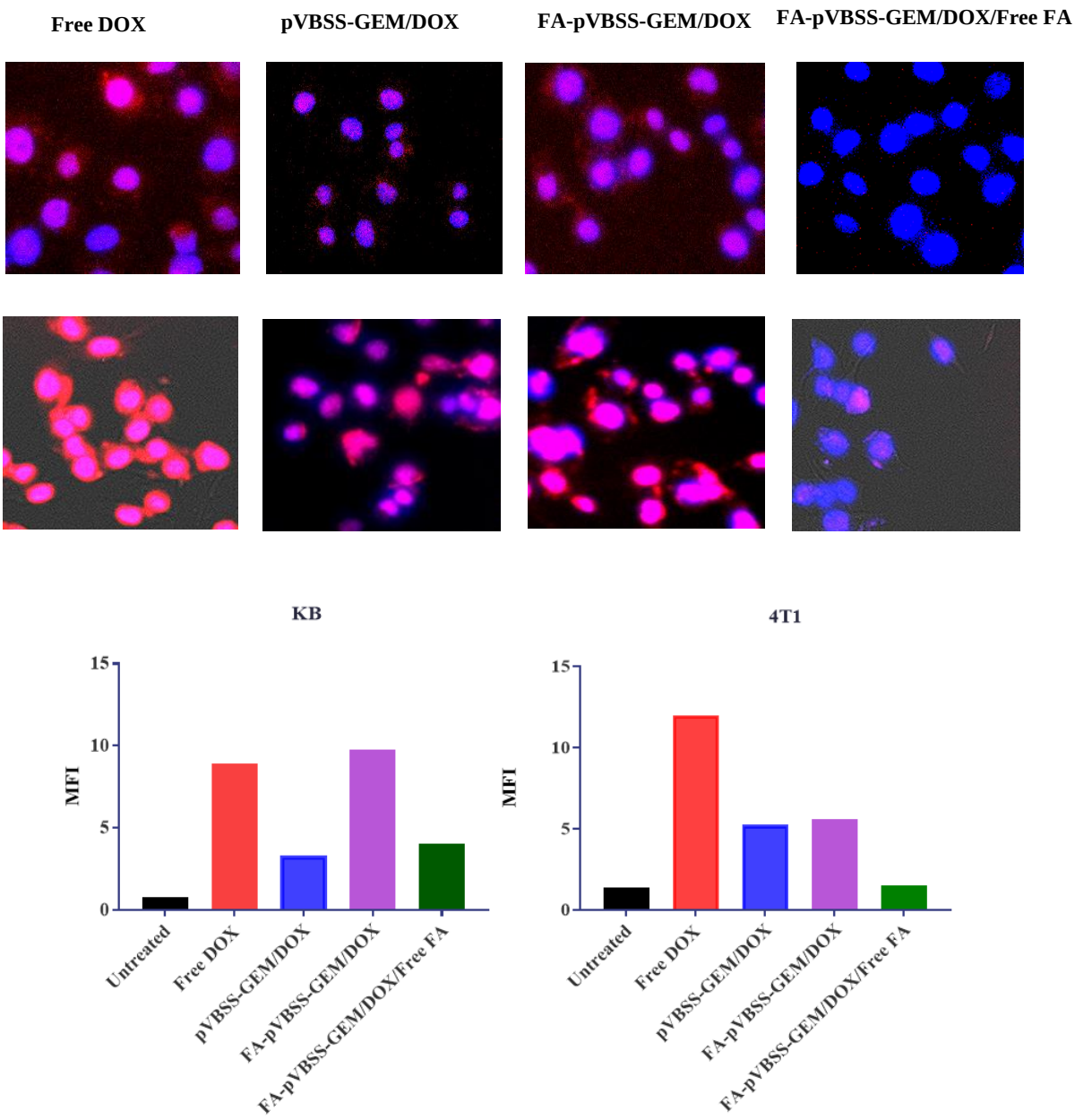

Figure 6: Cellular uptake of DOX as measured by (above) fluorescence microscopy and (below) flow cytometry

3.6 **Biodistribution of dox in vivo**

4T1.2 bearing Balb/c mice tumor tissues were used for biodistribution study. Figure 7 shows fluorescence images of tumor sections following 24-hour treatment with free DOX, pVBSS-GEM/DOX, and FA-pVBSS-GEM/DOX. Incorporation of DOX in both the micelle systems could substantially improve the tissue permeation, likely due to an increase in $t_{1/2}$. This is likely attributed to the extended circulation time of PEG-conjugated micelles and EPR effect. DOX uptake can be further increased by folate conjugated micelles, which have an active FR targeting potential in addition to passive EPR targeting. Coupling FA to micelle surface effectively retains the micellar DOX at tumor site due to the strong FA/FR interaction.

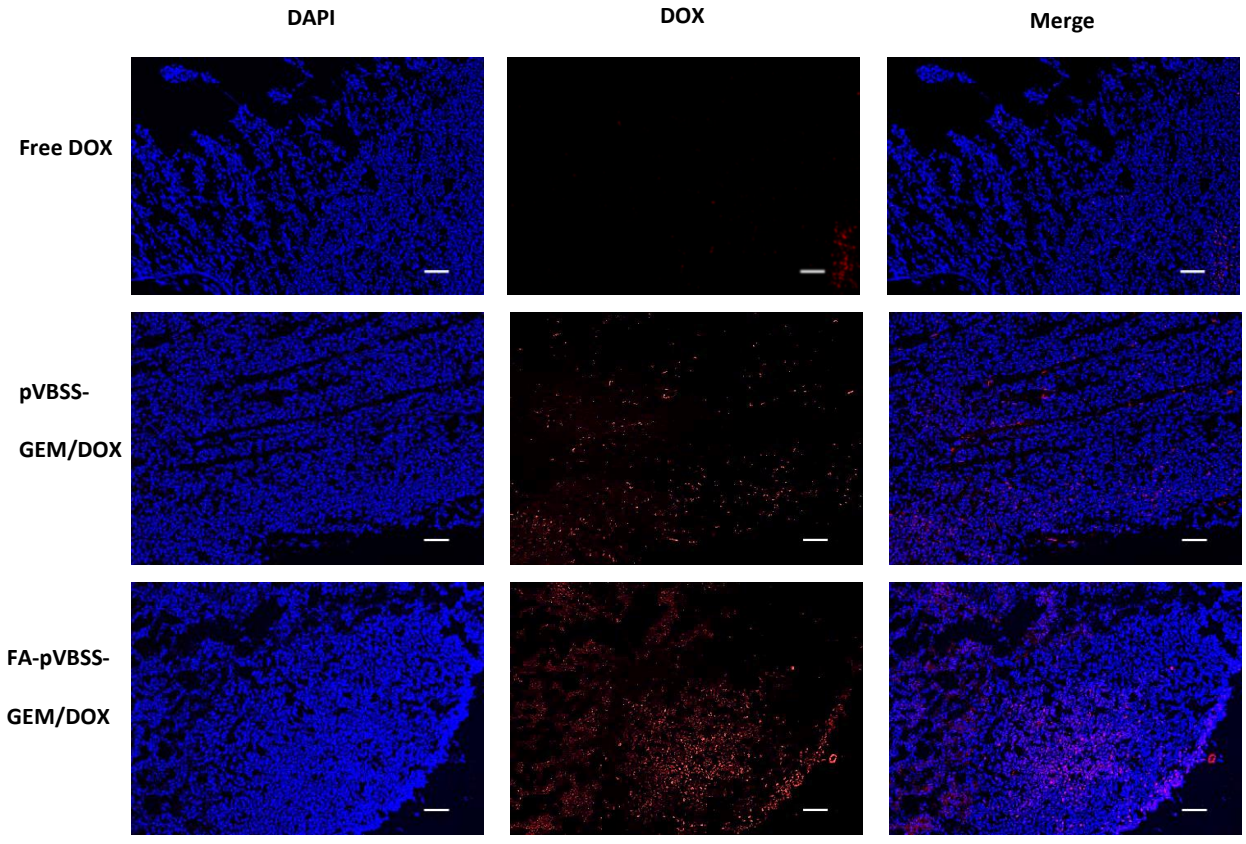

Figure 7: Uptake of DOX in 4T1.2 tumor tissue sections post 24 hours treatment

3.7 **In vivo near-infrared fluorescence (NIRF) optical imaging**

After confirming an increased uptake in the tumor microenvironment, we tested the biodistribution of micelle systems in other major organs in 4T1.2 bearing mouse, using DiR as a fluorescent probe. Free DiR, pVBSS-GEM/DiR, and FA-pVBSS-GEM/DiR were injected i.v., maintaining DiR concentration of 0.1 mg/kg in each formulation. Post 24 hours, the tumor and major organs from each group were excised and scanned using IVIS imaging. Figure 8 shows that free DiR is completely eliminated from the mice organs and delivering DiR via micelles has an enhanced permeability and retention benefit. DiR delivered via pVBSS-GEM/DOX system showed beneficial accumulation in tumor, but an even higher signal intensity was observed in liver and spleen. After introducing FA as a targeting ligand, the uptake of the micelle was highest in the tumor, and reduced in other organs. This observed evidence supports the fact that FA-pVBSS-GEM micelle can effectively deliver the probe to the tumor due to the FA/FR binding efficiency and reduce its uptake in other organs.

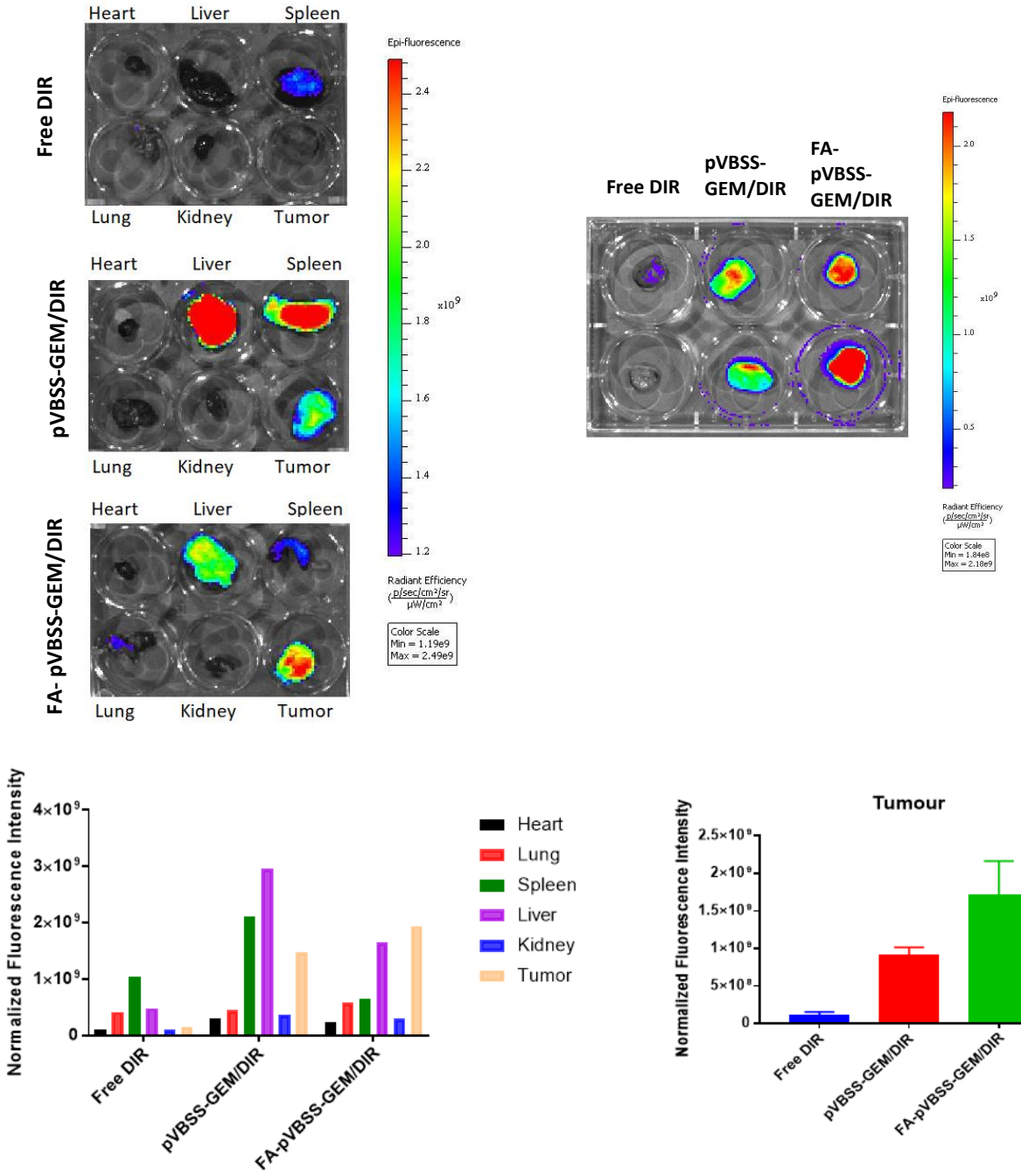

Figure 8: Biodistribution and accumulation of free and DiR loaded micelles in tumor and major organs

3.8 **In vivo antitumor efficacy study**

4T1.2 murine breast cancer model was chosen to study the in vivo therapeutic efficacy of DOX-loaded micelle systems. Saline was administered to the control group to mimic the natural growth of breast cancer and free DOX was used as a standard treatment control group. Tumor volume was measured to evaluate the efficacy of different groups and plotted in a growth curve as relative tumor volume (tumor volume at a given time point / initial tumor volume before 1st injection) (Figure 9). After a course of 16 days, free DOX-treated mice showed significantly smaller tumor as compared to the saline group ($p = 0.02$). Interestingly, compared to DOX, the blank carrier only pVBSS-GEM micelle itself showed a higher therapeutic efficacy, which can be attributed to the EPR effect of nanoparticles. Conjugating FA to blank carrier also improved the anti-tumor efficacy, however, it was not statistically significant. On loading DOX into the FA-pVBSS-GEM system, the therapeutic activity is further increased significantly ($p= 0.022$). This is due to the small size of micelles, active targeting and synergistic effect of the anticancer drugs administered. As depicted in the representational graph (Figure 10), the FA-pVBSS-GEM/DOX group showed the greatest IR of 85 ($\pm$ 5.5) %. Moreover, this group showed the smallest tumor size with average tumor weight of 0.37 g. During this study, no noticeable toxicity or significant body weight changes were observed in any treatment group.

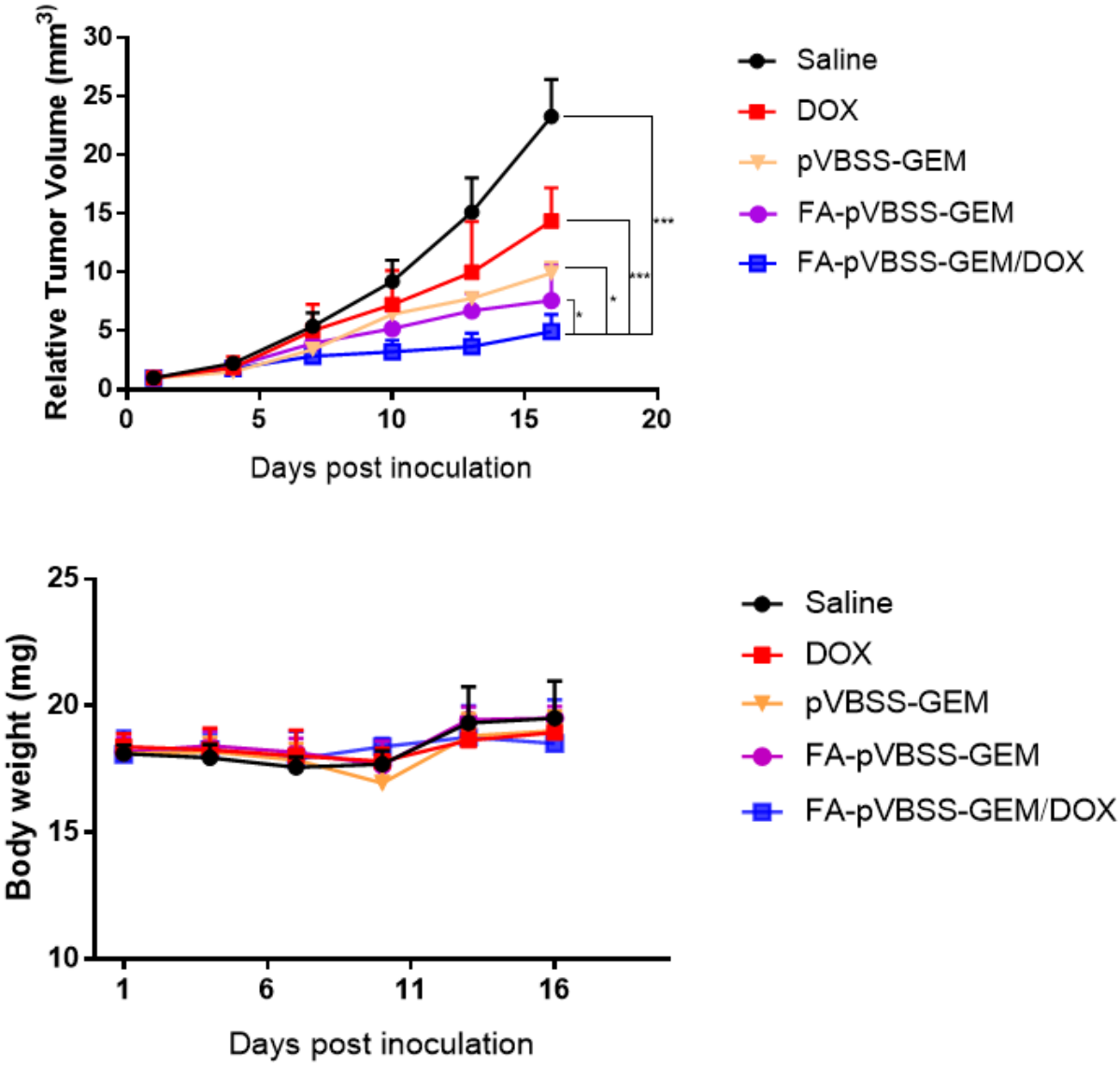

Figure 9: RTV and body weight monitored over 16 days in 4T1.2 breast cancer therapeutic study

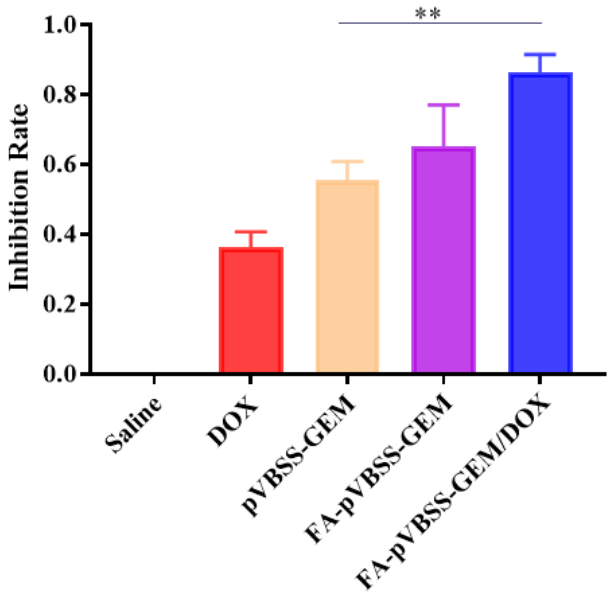

Figure 10: Inhibition rate of different treatment groups at day 16

3.8.1 **Safety evaluations**

After completing the therapeutic study, all the tumors and major body organs, along with blood serum were harvested. Several serum biological markers for liver/kidney function such as ALT and AST were examined for all groups. No liver toxicity was associated with the micelle and DOX-loaded micelle systems (Figure 11).

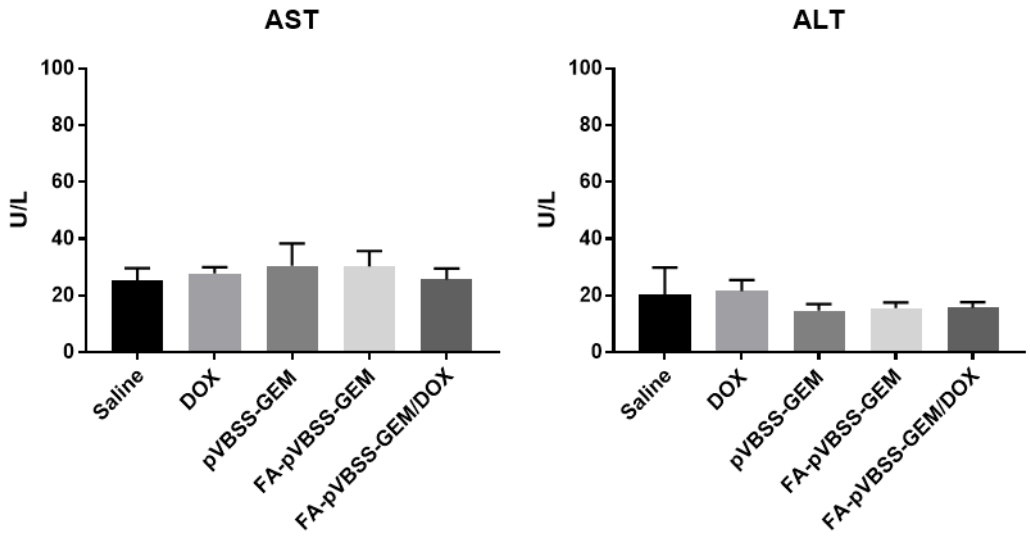

Figure 11: Serum AST and ALT enzyme activity in different treatment groups

The liver, kidney, lung, heart, spleen, and tumor of mice were harvested and embedded in parafilm blocks for histological analysis of tissue structure and damage (Figure 12). H&E stained tumor sections in the saline-treated group showed a typical high density of tumor cells with large nuclei. However, the histology of FA-pVBSS-GEM and FA-pVBSS-GEM/DOX showed bulk necrosis. Next, tumor sections were labeled by TUNEL reagents, to analyze tissue apoptosis. As expected, FA-pVBSS-GEM and FA-pVBSS-GEM/DOX showed the higher intensity of fluorescence, indicating more apoptotic cells. To further understand the proliferation of these tumor cells, Ki-67 protein staining was carried out. This protein is expressed explicitly in proliferating cells undergoing interphase and is not expressed in the G0 phase. Randomly, five different areas were selected and imaged for Ki-67 IHC and the staining was quantified using ImmuneRatio. FA-pVBSS-GEM/DOX treated tumor tissues exhibited the lowest level of Ki-67

expression, indicating significantly reduced cell proliferation compared with other treatments (Figure 13).

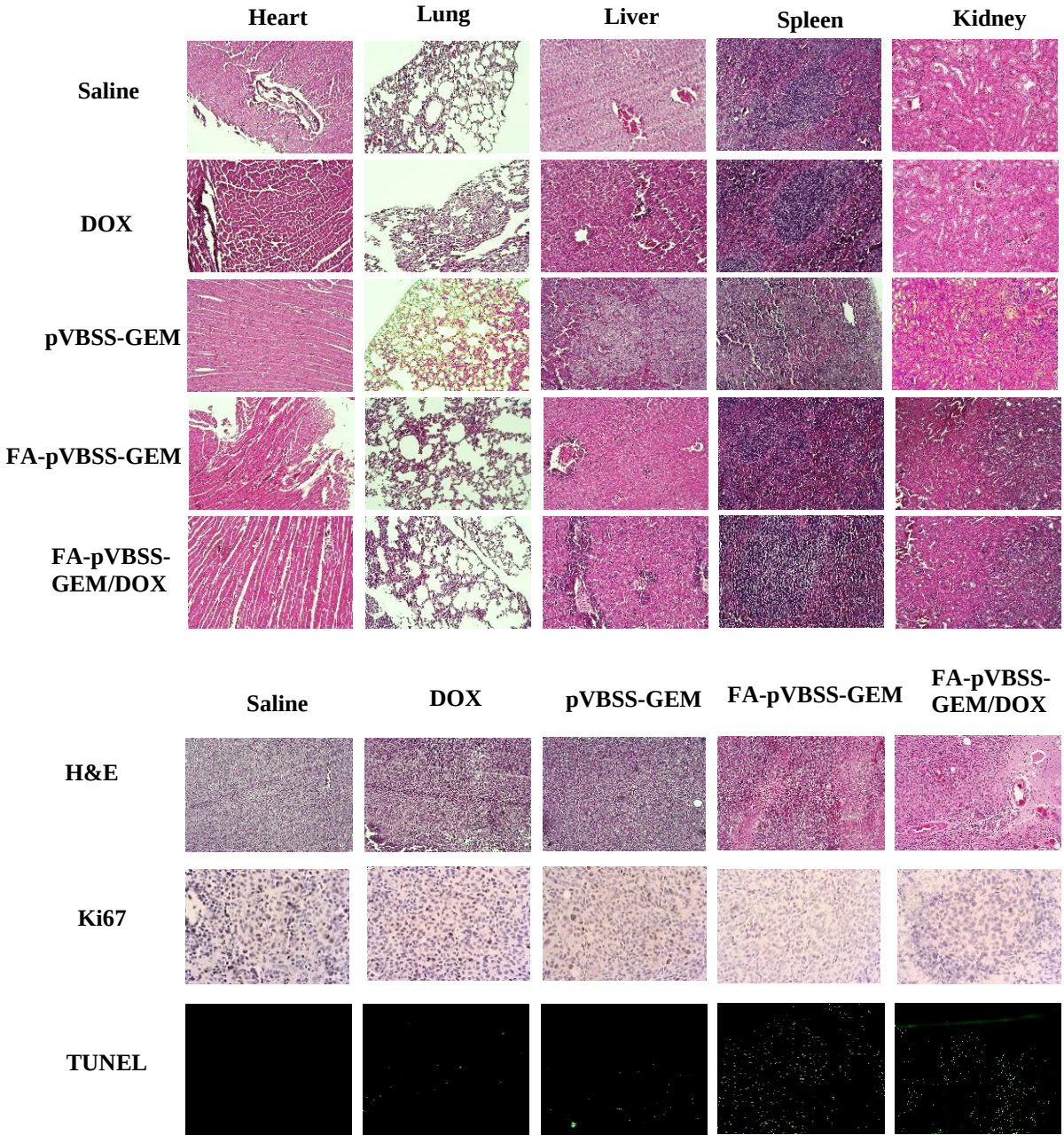

Figure 12: Safety/toxicity analysis of tumor and other major organs of different treatment groups

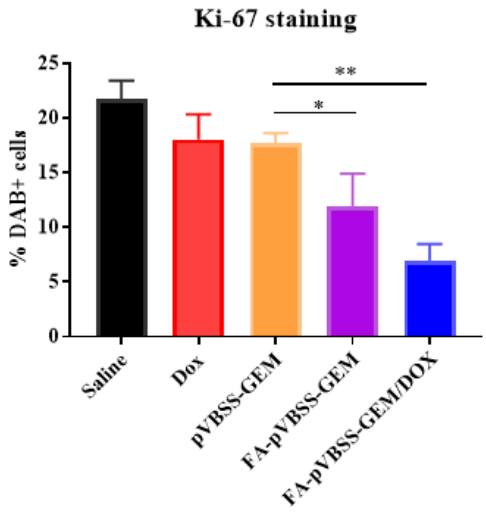

Figure 13: Ki-67 expression in tumor tissues of different treatment groups

3.9 **FRβ targeting in M2 macrophages**

Even though 4T1.2 does not overexpress FRα significantly, we still observe a benefit of targeting this tumor model in vivo, suggesting that there might be other cell types in the tumor microenvironment susceptible to our nanoparticle. To understand the targeting potential of this nanoparticle on specific M2 macrophage population. Macrophages from PBMC were isolated from mice spleen tissues and polarized towards M2 phenotype using IL 4 and IL 13 cytokines and the phenotype was tested by qPCR analyses. A dominant M2 phenotype was confirmed by a reduced iNOS and significantly higher Arg1 expression. We also confirmed an increase in Frβ expression in these polarized cells, further supporting that they can be targeted by FR targeting therapeutics (Figure 15).

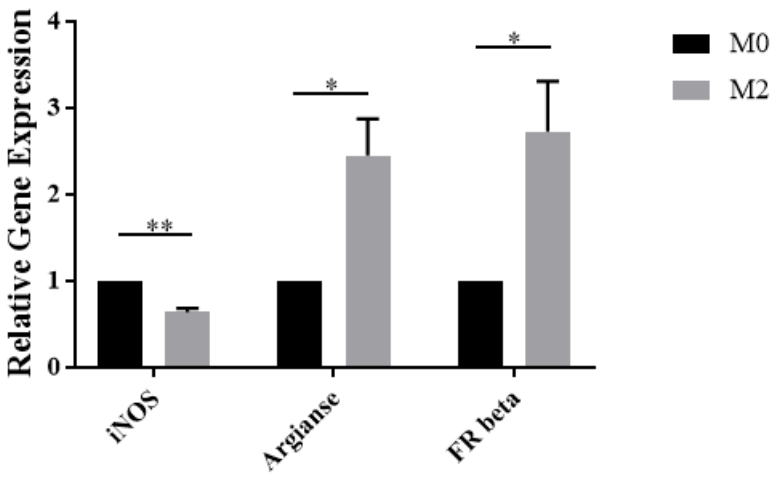

Figure 14: Gene expression profile for M0 and M2 macrophages

Next, the cellular uptake of DOX was analyzed on the M2 cells. For this, the cells were treated with free DOX, pVBSS-GEM/DOX, FA-pVBSS-GEM/DOX, and FA-pVBSS-GEM/DOX in the presence of 1 mM free folic acid for 30 min. The DOX concentration was maintained at 6 µg/mL. As seen in Figure 16, the binding of FA-pVBSS-GEM/DOX to M2 cells was obvious within 30 min of exposure. In contrast, pVBSS-GEM/DOX showed little cellular uptake at the same time of exposure. For free ligand competition study, free FA showed decreased uptake of DOX in M2 cells.

These results indicate that in the tumor microenvironment, FA-conjugated micelles could successfully target, and release GEM and DOX in cancer cells, as well as macrophages associated with tumor progression. This synergistic cytotoxic effect can significantly improve the therapeutic activity of our system.

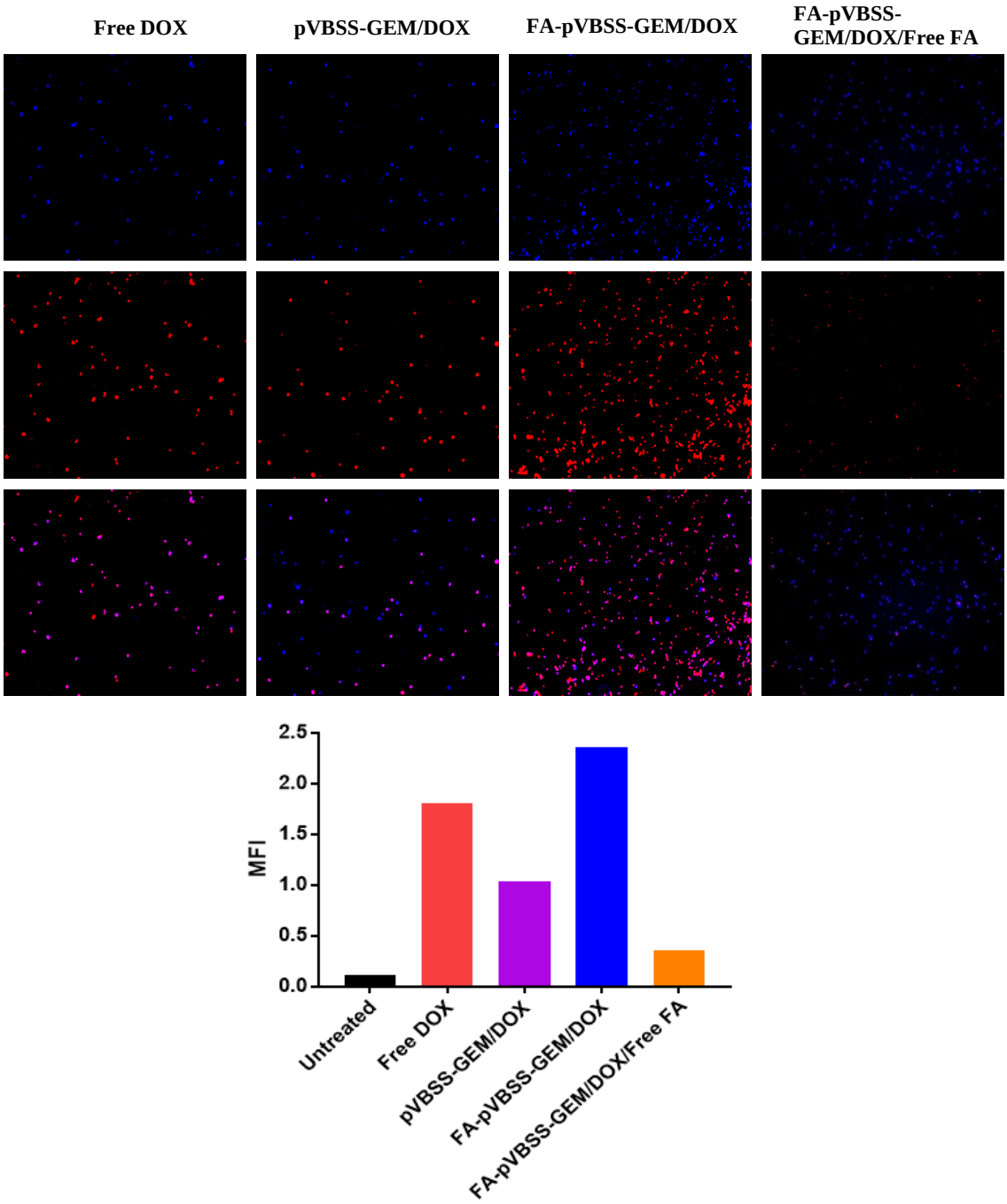

Figure 15: Cellular uptake of DOX in M2 cells

4.0 CONCLUSION

Overexpressed FRs in the tumor microenvironment are vulnerabilities that can be targeted by therapeutics to induce cancer cell death. In this project, we synthesized a polymeric micelle of diameter 10 nm for dual delivery of GEM and DOX. To improve the therapeutic activity of micelle at the tumor site and decrease its uptake in other organs, we conjugate FA to the surface as a targeting ligand. As expected, an increased uptake was observed in KB cells, which overexpress FR and this uptake was not significantly improved in 4T1.2 cells, which are known to have minimal overexpression of FR. Surprisingly, even though we do not see a clear advantage of the system in 4T1.2 by in vitro studies, results from NIRF imaging and therapeutic study reveal that FA-pVBSS-GEM/DOX successfully enhanced cellular uptake of micelles in vivo and significantly improved tumor regression in a 4T1.2 cancer model.

This paved the way for us to think about other cells present in the tumor microenvironment, which could potentially be targeted by our FA-conjugated micelle. Looking at the current findings of FR expression on the M2 population, we tested and confirmed an increased uptake of our micelle in these tumor-growth promoting macrophages. Thus, the observed anti-tumor effect of FA-pVBSS-GEM could be attributed to strong FA/FR interactions in the tumor microenvironment, as the system could successfully bind to FRα overexpressed on cancer cells and FRβ expressed on TAMs, giving a synergistic effect of both the cytotoxic drugs.

Appendix A : Abbreviations

Abbreviations:

ALT	Alanine Aminotransferase
Arg1	Arginase 1
AST	Aspartate Aminotransferase
CMC	Critical micellar concentration
DLS	Dynamix Light Scattering
DOX	Doxorubicin
EPR	Enhanced permeability and retention
FA	Folic Acid
FR	Folate receptor
GEM	Gemcitabine
GPCR	G protein-coupled receptors
H&E	Hematoxylin and eosin staining
IFNγ	Interferon gamma
IHC	Immunohistochemistry
iNOS	inducible nitric oxide synthase
IR	Inhibition rate
LPS	Lipopolysaccharide
PBS	Phosphate buffer solution
PDI	polydispersity index
PEG	Polyethylene glycol

PF	Primer forward
PR	Primer reverse
PTX	Paclitaxel
RT-qPCR	Reverse transcriptase PCR
RTV	Relative tumor volume
TAM	Tumor associated macrophages
TEM	Transmission electron microscopy
TUNEL	dUTP Nick-end Labeling

Appendix B : Chemicals

AIBN	Azobisisobutyronitrile
DCM	Dichloromethane
DIPEA	N,N- diisopropylethylamine
DiR	1,1’ -dioctadecyl-tetramethyl indotricarbocyanine iodide
DMSO	Dimethyl sulfoxide
EDC.HCl	1-ethyl -3-(3-dimethylaminopropyl)carbodiimide
HOBT	Hydroxybenzotriazole
K_2CO_3	Potassium Carbonate
MTT	(3-(4,5-dimethylthiazol-2-yl)-2,5-diphenyl tetrazolium bromide)
PE	Petroleum ether
THF	Tetrahydrofuran
TEA	Triethylamine

Bibliography

1. Siegel RL, Miller KD, Jemal A. Cancer Statistics, 2017. CA Cancer J Clin. 2017;67(1):7-30.
2. Chen Q, Zheng J, Yuan X, Wang J, Zhang L. Folic acid grafted and tertiary amino based pH-responsive pentablock polymeric micelles for targeting anticancer drug delivery. Mater Sci Eng C Mater Biol Appl. 2018;82:1-9.
3. Agudelo D, Bourassa P, Berube G, Tajmir-Riahi HA. Review on the binding of anticancer drug doxorubicin with DNA and tRNA: Structural models and antitumor activity. J Photochem Photobiol B. 2016;158:274-9.
4. Mizutani H, Tada-Oikawa S, Hiraku Y, Kojima M, Kawanishi S. Mechanism of apoptosis induced by doxorubicin through the generation of hydrogen peroxide. Life Sci. 2005;76(13):1439-53.
5. Du Y, Liang X, Li Y, Sun T, Jin Z, Xue H, et al. Nuclear and Fluorescent Labeled PD-1-Liposome-DOX-(64)Cu/IRDye800CW Allows Improved Breast Tumor Targeted Imaging and Therapy. Mol Pharm. 2017;14(11):3978-86.
6. Bea Pauwels MS, * Annelies E. C. Korst,Ph.D.,* Greet G. O. Pattyn,*, Hilde A. J. Lambrechts DRVB, Ph.D.,† Katrien Vermeulen,Ph.D.,† Marc Lenjou,† Christel M. J. De Pooter, M.D.,‡ Jan B. Vermorken, M.D.,* And Filip Lardon,Ph.D. Cell cycle effect of gemcitabine and its role in the radiosensitizing mechanism in vitro. Int J Radiation Oncology Biol Phys. 2003;57(4):1075–83.
7. Jingjing Sun a, Lingyi Sun b,1, Jianchun Li b, Jieni Xu a, Zhuoya Wana, Zubin Ouyang c, Lei Liang a, Song Li a,⇑, Dexing Zeng b,⇑. A multi-functional polymeric carrier for simultaneous positron emission tomography imaging and combination therapy. Acta Biomaterialia. 2018;75:312-22.
8. Jingjing Sun a b, c,1, Yichao Chen a,b,c,1,KeLi d,e,f, Yixian Huang a,b,c, Xiaofeng Fu g, Xiaolan Zhang a,b,c, Wenchen Zhao b, Yuan Wei a,b,c, Liang Xu d,e,f, Peijun Zhang g, Raman Venkataramanan b, Song Li a,b,c,⇑. A prodrug micellar carrier assembled from polymers with pendant farnesyl thiosalicylic acid moieties for improved delivery of paclitaxel. Acta Biomaterialia. 2016;43:282–91.
9. Kejun Jianga, Xu Songa,1, Liuqing Yanga, Lin Lia, Zhuoya Wanb, Xun Suna, Tao Gonga, Qing Lina,∗, ZZ, ∗. Enhanced antitumor and anti-metastasis efficacy against aggressive breast cancer with a fibronectin-targeting liposomal doxorubicin. Journal of Controlled Release. 2018;271:21-30.
10. Kwon SRCaGS. Polymeric Micelles for Drug Delivery. Current Pharmaceutical Design. 2006;12:4669-84.
11. Lu J, Huang Y, Zhao W, Chen Y, Li J, Gao X, et al. Design and characterization of PEG-derivatized vitamin E as a nanomicellar formulation for delivery of paclitaxel. Mol Pharm. 2013;10(8):2880-90.
12. Batrakova EV BT, Vetro JA, Kabanov AV. Polymer micelles as drug carriers. Imperial College Press. 2006:57-93.
13. Alibolandi M, Abnous K, Sadeghi F, Hosseinkhani H, Ramezani M, Hadizadeh F. Folate receptor-targeted multimodal polymersomes for delivery of quantum dots and doxorubicin

to breast adenocarcinoma: In vitro and in vivo evaluation. Int J Pharm. 2016;500(1-2):162-78.
14. Zhiliang Cheng AAZ, James Z. Hui, Vladimir R. Muzykantov, Andrew Tsourkas. Multifunctional Nanoparticles: Cost Versus Benefit of Adding Targeting and Imaging Capabilities. Science. 2012;338(6109):903–10.
15. Ao L, Wang B, Liu P, Huang L, Yue C, Gao D, et al. A folate-integrated magnetic polymer micelle for MRI and dual targeted drug delivery. Nanoscale. 2014;6(18):10710-6.
16. Biswas S, Kumari P, Lakhani PM, Ghosh B. Recent advances in polymeric micelles for anti-cancer drug delivery. Eur J Pharm Sci. 2016;83:184-202.
17. Wu B, Yu P, Cui C, Wu M, Zhang Y, Liu L, et al. Folate-containing reduction-sensitive lipid-polymer hybrid nanoparticles for targeted delivery of doxorubicin. Biomater Sci. 2015;3(4):655-64.
18. Wu D, Zheng Y, Hu X, Fan Z, Jing X. Anti-tumor activity of folate targeted biodegradable polymer-paclitaxel conjugate micelles on EMT-6 breast cancer model. Mater Sci Eng C Mater Biol Appl. 2015;53:68-75.
19. Zhang Y, Zhang H, Wu W, Zhang F, Liu S, Wang R, et al. Folate-targeted paclitaxel-conjugated polymeric micelles inhibits pulmonary metastatic hepatoma in experimental murine H22 metastasis models. Int J Nanomedicine. 2014;9:2019-30.
20. Yingjuan Lu PSL. Folate-mediated delivery of macromolecular anticancer therapeutic agents. Advanced Drug Delivery Reviews. 2012;64:342–52.
21. Anthony Cheung, 2 Heather J. Bax,#1,3 Debra H. Josephs,1,3 Kristina M. Ilieva,1,2 Giulia Pellizzari,1 James Opzoomer,1 Jacinta Bloomfield,1 Matthew Fittall,1,2 Anita Grigoriadis,2 Mariangela Figini,4 Silvana Canevari,4 James F. Spicer,3 Andrew N. Tutt, and Sophia N. Karagiannis1,2. Targeting folate receptor alpha for cancer treatment. Oncotarget. 2016;7(32):52553–74.
22. Eun Seong Lee KN, You Han Bae. Polymeric micelle for tumor pH and folate-mediated targeting. Journal of Controlled Release. 2003;91(1-2):103–13.
23. Chen H, Ahn R, Van den Bossche J, Thompson DH, O'Halloran TV. Folate-mediated intracellular drug delivery increases the anticancer efficacy of nanoparticulate formulation of arsenic trioxide. Mol Cancer Ther. 2009;8(7):1955-63.
24. Bahrami B, Mohammadnia-Afrouzi M, Bakhshaei P, Yazdani Y, Ghalamfarsa G, Yousefi M, et al. Folate-conjugated nanoparticles as a potent therapeutic approach in targeted cancer therapy. Tumour Biol. 2015;36(8):5727-42.
25. Jiayin Shen1 YH, 2, Karson S. Putt2, Sunil Singhal3 W. Visscher5, Linda M. Murphy6 and Philip S. Low1,2, Haiyong Han4 , Daniel. Assessment of folate receptor alpha and beta expression in selection of lung and pancreatic cancer patients for receptor targeted therapies. Oncotarget. 2018;9(4):4485-95.
26. Low PS, Kularatne SA. Folate-targeted therapeutic and imaging agents for cancer. Curr Opin Chem Biol. 2009;13(3):256-62.
27. Lu T, Sun J, Chen X, Zhang P, Jing X. Folate-conjugated micelles and their folate-receptor-mediated endocytosis. Macromol Biosci. 2009;9(11):1059-68.
28. Yoo HS, Park TG. Folate receptor targeted biodegradable polymeric doxorubicin micelles. J Control Release. 2004;96(2):273-83.
29. Butt AM, Mohd Amin MC, Katas H. Synergistic effect of pH-responsive folate-functionalized poloxamer 407-TPGS-mixed micelles on targeted delivery of anticancer drugs. Int J Nanomedicine. 2015;10:1321-34.

30. Jisha J. Pillai AKTT, Ruby John Anto,b Nandan C. Devika,a N. Ashwanikumara and G. S. Vinod Kumar. Curcumin entrapped folic acid conjugated PLGA– PEG nanoparticles exhibit enhanced anticancer activity by site specific delivery. RSC Adv. 2015;5(43):25518–24.
31. Luong D, Kesharwani P, Alsaab HO, Sau S, Padhye S, Sarkar FH, et al. Folic acid conjugated polymeric micelles loaded with a curcumin difluorinated analog for targeting cervical and ovarian cancers. Colloids Surf B Biointerfaces. 2017;157:490-502.
32. Varshosaz J, Hassanzadeh F, Sadeghi Aliabadi H, Nayebsadrian M, Banitalebi M, Rostami M. Synthesis and characterization of folate-targeted dextran/retinoic acid micelles for doxorubicin delivery in acute leukemia. Biomed Res Int. 2014;2014:525684.
33. Yang L, Li J, Zhou W, Yuan X, Li S. Targeted delivery of antisense oligodeoxynucleotides to folate receptor-overexpressing tumor cells. J Control Release. 2004;95(2):321-31.
34. Hami Z, Amini M, Ghazi-Khansari M, Rezayat SM, Gilani K. Doxorubicin-conjugated PLA-PEG-Folate based polymeric micelle for tumor-targeted delivery: Synthesis and in vitro evaluation. DARU Journal of Pharmaceutical Sciences. 2014;22(1):30.
35. Varshosaz J, Taymouri S, Hassanzadeh F, Javanmard SH, Rostami M. Folated synperonic-cholesteryl hemisuccinate polymeric micelles for the targeted delivery of docetaxel in melanoma. Biomed Res Int. 2015;2015:746093.
36. Wen Zhou, ‡ Xing Yuan,†,‡ Annette Wilson,§ Lijuan Yang,†,‡ Michael Mokotoff,‡ Bruce Pitt,§ and Song Li. Efficient Intracellular Delivery of Oligonucleotides Formulated in Folate Receptor-Targeted Lipid Vesicles. Bioconjugate Chemistry. 2002;2002:1220−5.
37. Gao ZG, Tian L, Hu J, Park IS, Bae YH. Prevention of metastasis in a 4T1.2 murine breast cancer model by doxorubicin carried by folate conjugated pH sensitive polymeric micelles. J Control Release. 2011;152(1):84-9.
38. Li M, Liu Y, Feng L, Liu F, Zhang L, Zhang N. Polymeric complex micelles with double drug-loading strategies for folate-mediated paclitaxel delivery. Colloids Surf B Biointerfaces. 2015;131:191-201.
39. Lv Y, Yang B, Jiang T, Li YM, He F, Zhuo RX. Folate-conjugated amphiphilic block copolymers for targeted and efficient delivery of doxorubicin. Colloids Surf B Biointerfaces. 2014;115:253-9.
40. Qiu LY, Yan L, Zhang L, Jin YM, Zhao QH. Folate-modified poly(2-ethyl-2-oxazoline) as hydrophilic corona in polymeric micelles for enhanced intracellular doxorubicin delivery. Int J Pharm. 2013;456(2):315-24.
41. Yang C, Chen H, Zhao J, Pang X, Xi Y, Zhai G. Development of a folate-modified curcumin loaded micelle delivery system for cancer targeting. Colloids Surf B Biointerfaces. 2014;121:206-13.
42. Zelai He, 2 Jingwen Huang,2 Yuanyuan Xu,3 Xiangyu Zhang,3 Yanwei Teng,3 Can Huang,3 Yufeng Wu,4 Xi Zhang,2 Huijun Zhang,5 and Wenjie Sun1. Co-delivery of cisplatin and paclitaxel by folic acid conjugated amphiphilic PEG-PLGA copolymer nanoparticles for the treatment of non-small lung cancer. Oncotarget. 2015;6(39):42150–68.
43. Qiao J, Dong P, Mu X, Qi L, Xiao R. Folic acid-conjugated fluorescent polymer for up-regulation folate receptor expression study via targeted imaging of tumor cells. Biosens Bioelectron. 2016;78:147-53.
44. de Boer E, Crane LM, van Oosten M, van der Vegt B, van der Sluis T, Kooijman P, et al. Folate Receptor-Beta Has Limited Value for Fluorescent Imaging in Ovarian, Breast and Colorectal Cancer. PLoS One. 2015;10(8):e0135012.

45. O'Shannessy DJ, Somers EB, Wang LC, Wang H, Hsu R. Expression of folate receptors alpha and beta in normal and cancerous gynecologic tissues: correlation of expression of the beta isoform with macrophage markers. J Ovarian Res. 2015;8:29.
46. Davis MJ, Tsang TM, Qiu Y, Dayrit JK, Freij JB, Huffnagle GB, et al. Macrophage M1/M2 polarization dynamically adapts to changes in cytokine microenvironments in Cryptococcus neoformans infection. MBio. 2013;4(3):e00264-13.
47. Jian Ming Hu1 SGL, Kai Liu1 , Ji Hong Liu1 , Xian Li Jiang1 , Hong Zou1, Li Juan Pang1 , Xue Li Wang1 , Chun Xia Liu1 , Xiao Bin Cui1 Zhao1, Xi Hua Shen1, Jin Fang Jiang1, Wei Hua Liang1, Xiang Lin Yuan3, Yun Zhao Chen1 , Lan Yang1 , Feng Li1,2, , Jin. CD163 as a marker of M2 macrophage, contribute to predict aggressiveness and prognosis of Kazakh esophageal squamous cell carcinoma. Oncotarget. 2017;8(13):21526-38.
48. Feng Y, Shen J, Streaker ED, Lockwood M, Zhu Z, Low PS, et al. A folate receptor beta-specific human monoclonal antibody recognizes activated macrophage of rheumatoid patients and mediates antibody-dependent cell-mediated cytotoxicity. Arthritis Res Ther. 2011;13(2):R59.
49. Puig-Kroger A, Sierra-Filardi E, Dominguez-Soto A, Samaniego R, Corcuera MT, Gomez-Aguado F, et al. Folate receptor beta is expressed by tumor-associated macrophages and constitutes a marker for M2 anti-inflammatory/regulatory macrophages. Cancer Res. 2009;69(24):9395-403.
50. Nagai T, Tanaka M, Tsuneyoshi Y, Xu B, Michie SA, Hasui K, et al. Targeting tumor-associated macrophages in an experimental glioma model with a recombinant immunotoxin to folate receptor beta. Cancer Immunol Immunother. 2009;58(10):1577-86.
51. Mia S, Warnecke A, Zhang XM, Malmstrom V, Harris RA. An optimized protocol for human M2 macrophages using M-CSF and IL-4/IL-10/TGF-beta yields a dominant immunosuppressive phenotype. Scand J Immunol. 2014;79(5):305-14.